A simple biomineralization model to explain Li, Mg, and Sr incorporation into aragonitic foraminifera and corals

T.M. Marchitto, P. Bryan, W. Doss, M.T. Mcculloch, P. Montagna

A simple biomineralization model to explain Li, Mg, and Sr incorporation into aragonitic foraminifera and corals

T. M. Marchitto[a,b,*], S. P. Bryan[c], W. Doss[d], M. T. McCulloch[e], P. Montagna[f,g]

[a] *Department of Geological Sciences, University of Colorado, Boulder, CO 80309, USA*

[b] *Institute of Arctic and Alpine Research, University of Colorado, Boulder, CO 80309, USA*

[c] *Department of Geosciences, Colorado State University, Fort Collins, CO 80523, USA*

[d] *Institut Universitaire Européen de la Mer, Université de Bretagne Occidentale, 29280 Plouzané, France*

[e] *School of Earth and Environment, The University of Western Australia, Crawley, WA 6009, Australia*

[f] *Istituto di Scienze Marine, Consiglio Nazionale delle Ricerche, I-40129 Bologna, Italy*

[g] *Laboratoire des Sciences du Climat et de l'Environnement LSCE/IPSL, 91198 Gif-sur-Yvette, France*

*Corresponding author. E-mail: tom.marchitto@colorado.edu

Abstract

In contrast to Li/Ca and Mg/Ca, Li/Mg is strongly anticorrelated with growth temperature in aragonites precipitated by the benthic foraminifer *Hoeglundina elegans* and a wide range of scleractinian coral taxa. We propose a simple conceptual model of biomineralization that explains this pattern and that is consistent with available abiotic aragonite partition coefficients. Under this model the organism actively modifies seawater within its calcification pool by raising

its [Ca^{2+}], using a pump that strongly discriminates against both Li^{+} and Mg^{2+}. Rayleigh fractionation during calcification effectively reverses this process, removing Ca^{2+} while leaving most Li^{+} and Mg^{2+} behind. The net effect of these two processes is that Li/Mg in the calcifying fluid remains very close to the seawater value, and temperature-dependent abiotic partition coefficients are expressed in the biogenic aragonite Li/Mg ratio. We further show that coral Sr/Ca is consistent with this model if the Ca^{2+} pump barely discriminates against Sr^{2+}. In *H. elegans* the covariation of Sr/Ca and Mg/Ca requires either that the pump more strongly discriminates against Sr^{2+}, or that cation incorporation is affected by aragonite precipitation rate via the mechanism of surface entrapment. In either case Li/Mg is minimally affected by such 'vital effects' which plague other elemental ratio paleotemperature proxies.

Keywords: biomineralization; Li/Ca; Mg/Ca; Sr/Ca; paleotemperature proxies

1. Introduction

Dissolved Li, Mg, Sr, and Ca all behave nearly conservatively in seawater, meaning that their ratios are approximately constant throughout the oceans. The oceanic residence times of these four elements are relatively long, on the order of 1 to 10 Ma, so that oceanic metal/Ca ratios are also relatively constant through time during the late Quaternary. Hence any changes in the metal/Ca of biogenic $CaCO_3$ may potentially be attributed to variations in the environmental parameter(s) that affect metal partitioning into the mineral, such as temperature. Mg/Ca has been widely applied as a paleotemperature proxy in calcitic foraminifera (Nürnberg, 1995), while Sr/Ca has been similarly used in aragonitic corals (Beck et al., 1992). In both cases ancillary environmental parameters such as carbonate saturation state, and/or physiological parameters

such as growth rate, often appear to overprint the temperature signal. For the ratios that are not widely used as paleotemperature proxies, Sr/Ca in foraminifera and Mg/Ca in corals, such ancillary effects likely obscure any temperature dependence. Improved characterization of the various influences on metal partitioning is therefore a crucial goal of paleoceanographic proxy development, with an eye toward greater understanding of the biomineralization process.

Following the pioneering work of Delaney et al. (1985), Li/Ca has received renewed attention in both foraminifera and corals, but has not yet seen widespread application as a paleoceanographic proxy. Several studies have demonstrated a negative correlation between biogenic Li/Ca and temperature, but significant ancillary influences such as calcification rate have also been suggested (e.g. Hall and Chan, 2004; Hathorne et al., 2013; Marriott et al., 2004a, 2004b). Benthic foraminiferal Li/Ca from a holothermal depth transect is positively correlated with seawater saturation state with respect to calcite (Lear and Rosenthal, 2006), leading to the suggestion that Mg/Ca and Li/Ca can be used in linear combination to solve for both paleotemperature and saturation state (Lear et al., 2010). Bryan and Marchitto (2008) showed that Mg/Li in several taxa of benthic foraminifera is better correlated to temperature than either Mg/Ca or Li/Ca alone, especially for the aragonitic *Hoeglundina elegans* (r^2=0.49 for Mg/Ca, 0.90 for Mg/Li). They proposed that both Mg/Ca and Li/Ca reflect, in part, modification of the internal calcification pool, and that the ratio Mg/Li effectively corrects for physiological and/or saturation state influences, thereby isolating the temperature effect. A similar improvement using Mg/Li (or Li/Mg) has since been demonstrated in a diverse range of aragonitic corals, including deep sea taxa (Case et al., 2010; Montagna et al., 2014; Raddatz et al., 2013).

Here we further explore the relationship between Li/Ca and Mg/Ca in biogenic aragonites, and use it to construct a simple model of biomineralization. We then discuss the implications of that model for the coral Sr/Ca paleotemperature proxy.

2. Materials and methods

We present 11 new metal/Ca ratios in *H. elegans* from nine Holocene core tops (Table 1). Each sample contained ~5-10 individuals >250 μm, which were crushed and reductively and oxidatively cleaned following the methods of Boyle and Rosenthal (1996). Samples were analyzed for a suite of trace and minor elemental ratios by high-resolution sector field ICP-MS, as described by Marchitto (2006). Long-term 1σ precision is 0.9% for Li/Ca, 0.5% for Mg/Ca, and 0.6% for Sr/Ca. Concentrations of contaminant elements Al, Fe, and Mn were all negligible. We also report 34 previously unpublished *H. elegans* Sr/Ca ratios from the Florida Straits core tops measured for Li/Mg by Bryan and Marchitto (2008) (Table S1), analyzed using the methods described above; and 19 previously unpublished Sr/Ca ratios from a subset of the fibrous Li/Mg samples presented in Montagna et al. (2014) (Table S2), measured by laser ablation quadrupole ICP-MS following the methods of Montagna et al. (2007), with a 1σ precision of 1.6% based on a *Porites* external standard.

Published core top *H. elegans* Li/Ca and Mg/Ca results are compiled from Hall and Chan (2004) and Bryan and Marchitto (2008). Hall and Chan (2004) Mg/Ca is corrected downward by the 15% laboratory offset noted by Rosenthal et al. (2006). We omit one *H. elegans* measurement from Bryan and Marchitto (2008) that has a much different Li/Mg value than its replicate; and further reject one new sample that is a 3σ outlier from an exponential fit of Li/Mg versus temperature (Table 1). Modern coral Li/Ca and Mg/Ca data are compiled from Case et al.

(2010), Hathorne et al. (2013), Montagna et al. (2014), Raddatz et al. (2013), and Fowell et al. (2016). The interpolated monthly Hathorne et al. (2013) data (excluding the anomalous 1979-80 interval, as in that study), and the monthly to bi-monthly Fowell et al. (2016) data, are binned into 3°C quasi-seasonal groups based on sea surface temperature at the time of formation, to prevent individual specimens from exerting undue influence on regressions. For Montagna et al. (2014) we plot all of their solution-based measurements, plus laser ablation measurements (on fibrous aragonite) from corals where solution measurements were not made; they found no significant difference between the two methods when performed on the same corals. Among the compiled coral data we omit the two samples that Case et al. (2010) flagged as 'chalky' and chemically anomalous; and further reject two 3σ Li/Mg outliers as was done for *H. elegans*. *H. elegans* paired Mg/Ca and Sr/Ca data are compiled from Hall and Chan (2004) and Rosenthal et al. (2006). Coral paired Mg/Ca and Sr/Ca data are compiled from Allison and Finch (2010), López Correa et al. (2010), Gagnon et al. (2007), Inoue et al. (2007), Montagna et al. (2007), Reynaud et al. (2007), Shirai et al. (2005), Wei et al. (2000), and Xiao et al. (2014).

3. Results and discussion

3.1. Li/Ca, Mg/Ca, and Li/Mg versus temperature

With the addition of new measurements from the deep sea, the weak negative correlation between Li/Ca and temperature reported for *H. elegans* (Bryan and Marchitto, 2008; Hall and Chan, 2004) becomes even weaker (r^2=0.01, Fig 1a). Aragonitic coral Li/Ca exhibits a considerably stronger negative correlation to temperature (r^2=0.52 across multiple taxa, Fig. 1a), as has been noted previously (Case et al., 2010; Montagna et al., 2014). For Mg/Ca in *H. elegans* the correlation to temperature (positive) is much better than for Li/Ca (r^2=0.69), but across coral

taxa Mg/Ca is slightly worse than Li/Ca (r^2=0.36). Li/Mg ratios are not only much better correlated to temperature than either Li/Ca or Mg/Ca, but the relationship across coral taxa is remarkably similar to that for *H. elegans* (Hathorne et al., 2013) (Fig. 1c). The best fits are exponential decay functions:

$$\textit{H. elegans}: \text{Li/Mg} = 5.43\pm0.11e^{-0.0551\pm0.0024T} \quad (r^2 = 0.91) \quad (1)$$

$$\text{corals: Li/Mg} = 5.29\pm0.06e^{-0.0475\pm0.0013T} \quad (r^2 = 0.96) \quad (2)$$

$$\textit{H. elegans} \text{ and corals: Li/Mg} = 5.34\pm0.06e^{-0.0502\pm0.0012T} \quad (r^2 = 0.94) \quad (3)$$

where temperature (T) is in °C. The exponents on these equations indicate a decrease in Li/Mg of roughly 5% per °C, similar to the values reported by Hathorne et al. (2013) (4.92%), Montagna et al. (2014) (4.9%), and Fowell et al. (2016) (5%), each based on subsets of the data compiled here. That the Li/Mg chemistry of aragonite produced by cnidarians behaves so similarly to that precipitated by protozoa suggests that this ratio is controlled predominantly by temperature dependent thermodynamic processes, rather than the taxon-specific physiological 'vital effects' that appear to impact Li/Ca and Mg/Ca. Note that different genera of calcitic benthic foraminifera do not exhibit such uniformity (Bryan and Marchitto, 2008), nor do planktonic foraminifera (Allen et al., 2016), so our model does not apply directly to them (see Section 3.6).

Additional insight into this aragonite Li/Mg behavior may be gained by plotting Li/Ca against Mg/Ca (Fig. 2). Within a given temperature bin (color-coded in Fig. 2), *H. elegans* exhibits a range of Li/Ca and Mg/Ca values, but they plot as an array along a line that, if forced through the origin, represents constant Li/Mg (Fig. 2a). The slopes of those lines decrease as temperature increases, reflecting the decrease of Li/Mg with temperature discussed above. The various coral taxa behave in the same way, with generally higher Li/Ca and Mg/Ca ratios but similar Li/Mg compared to *H. elegans* (Fig. 2b). This may also help to illustrate why Li/Ca is

more strongly correlated to temperature in warm waters (e.g. Hathorne et al., 2013) than in cold waters (e.g. Case et al., 2010): all else being equal, the shallower slopes of the warm-end lines result in smaller Li/Ca ranges at a given temperature than do the steeper cold-end lines (Fig. 2b).

3.2. Comparison to abiotic partition coefficients

We suggest that the slopes of the lines in Figure 2 are set by the ratios between the temperature-dependent abiotic partition coefficients $K_{Li/Ca}$ and $K_{Mg/Ca}$, and that the spread along each line results from varying calcification rates (Section 3.3) and/or the organisms' modifications of their calcifying fluids (Sections 3.4-3.5). Constraints on abiotic aragonite $K_{Mg/Ca}$ as a function of temperature are provided by the inorganic precipitation experiments of Gaetani and Cohen (2006), who found an exponential decrease with temperature (r^2=0.996). Gaetani and Cohen (2006) noted that their $K_{Sr/Ca}$ results agreed well with values from Kinsman and Holland (1969), who used the same experimental approach. We make no assumption that these partition coefficients reflect substitution for Ca^{2+}, and indeed Mg^{2+} does not appear to occupy the Ca^{2+} lattice site in abiotic or coral aragonite (Finch and Allison, 2007; 2008).

If we assume that the Gaetani and Cohen (2006) $K_{Mg/Ca}$ values are applicable to biogenic aragonite, then we can combine them with the data in Figure 2b to predict abiotic $K_{Li/Ca}$ as a function of temperature. For each temperature bin, we first find the predicted $K_{Mg/Ca}$ at the central temperature using Gaetani and Cohen's (2006) temperature dependence. We then combine that coefficient with seawater Mg/Ca to predict an aragonite Mg/Ca, which would be the mineral's ratio if it were precipitated directly from unmodified seawater. Since modification of the organism's calcifying fluid hypothetically results in movement along the Li/Mg isotherm without changing its slope, the slope can be multiplied by the calculated aragonite Mg/Ca to

160 predict the corresponding aragonite Li/Ca if precipitated from unmodified seawater.
161 Combination of that value with seawater Li/Ca yields $K_{Li/Ca}$. This analysis suggests that abiotic
162 $K_{Li/Ca}$ should decrease exponentially by ~7% per °C:

163 $$K_{Li/Ca} = 0.0252 \pm 0.0002 e^{-0.0707 \pm 0.0011 T} \quad (4)$$

164 with $r^2 = 0.999$ (Fig. 3). This temperature sensitivity is close to that calculated by Montagna et al.
165 (2014) using a similar approach (~6.7% per °C). We are not aware of any abiotic aragonite
166 precipitation experiments that determine $K_{Li/Ca}$ as a function of temperature. Marriott et al.
167 (2004a) did, however, make two abiotic aragonite determinations at 25°C (and near-seawater
168 salinities) that are within 30% of our predicted value (Fig. 3). $K_{Li/Ca}$ in abiotic calcite decreases
169 by ~5% per °C (r^2=0.995) (Marriott et al., 2004b) with values that are comparable to our
170 aragonite predictions (Fig. 3). We note that at 25°C the difference in calcite $K_{Li/Ca}$ between the
171 two Marriott et al. studies is even larger than between Marriott et al.'s (2004a) aragonite $K_{Li/Ca}$
172 and our prediction, so the latter discrepancy may be insignificant. In summary, our predicted
173 abiotic aragonite $K_{Li/Ca}$ temperature dependence awaits experimental confirmation, but available
174 data suggest that our derived values are reasonable.
175
176 **3.3. Hypothetical effect of precipitation rate**
177 Gaetani and Cohen (2006) noted that their abiotic aragonite $K_{Mg/Ca}$, $K_{Sr/Ca}$, and $K_{Ba/Ca}$ values
178 were all substantially larger than predicted from thermodynamic equilibrium according to lattice
179 strain theory. They proposed that the observations could be explained by surface entrapment
180 during crystal growth (Watson, 2004), with reduced entrapment at higher temperatures due to
181 higher ionic diffusivities in the lattice surface. This model also predicts a positive dependence on
182 precipitation rate, which is borne out for Mg and U in aragonite precipitation experiments:

183 apparent entrapment varies from zero to 100% (relative to the temperature-dependent limit) over
184 about three orders of magnitude in growth rate (Gabitov et al., 2008). This raises a potential
185 complication for applying the Gaetani and Cohen (2006) $K_{Mg/Ca}$ results to biogenic aragonite: if
186 either their experimental precipitation rates or biogenic precipitation rates are substantially below
187 the levels at which entrapment asymptotes at 100%, then the two are not directly comparable.
188 Gaetani and Cohen's (2006) precipitation rates were apparently above the level of ~100%
189 Mg entrapment as measured by Gabitov et al. (2008). However, the Mg/Ca and Li/Ca ratios
190 measured in *H. elegans* and in corals are substantially lower than predicted in Section 3.2 for
191 aragonite precipitated from unmodified seawater (black dots in Fig. 4). This could mean that
192 biogenic $K_{Mg/Ca}$ and $K_{Li/Ca}$ are each decreased by a range of lower precipitation rates and less
193 surface entrapment, with zero-entrapment Mg/Ca and Li/Ca values occurring somewhere close to
194 the origin in Figure 4 (note that lattice strain theory calculations are exceedingly sensitive to
195 ionic radii, which are not well known at the 9-coordination of aragonite, so we do not plot the
196 zero entrapment equilibrium values). Microscale measurements of linear extension rates in some
197 fibrous ('wall') portions of the *Pocillopora damicornis* skeleton (Brahmi et al., 2012) appear to
198 be lower (~0.05-0.2 nm s^{-1}) than Gabitov et al.'s (2008) 100% entrapment threshold (~0.2 nm s^{-1}
199 or higher), implying that kinetics may be important in corals. Centers of calcification (COCs, or
200 'rapid accretion deposits') grow faster (Brahmi et al., 2012), and their elevated Li/Ca and Mg/Ca
201 ratios (by roughly a factor of two) have been attributed to greater entrapment (Montagna et al.,
202 2014; Rollion-Bard and Blamart, 2015).
203 If this interpretation is correct, the minimal Li/Mg deviations away from isotherms (Figs. 2,
204 4a) require that the *ratio* between the two partition coefficients remains nearly constant at a
205 given temperature as precipitation rates vary (i.e. that $K_{Li/Ca}$ and $K_{Mg/Ca}$ have approximately the

same sensitivity to precipitation rate). Providing some support for this scenario, Gabitov et al. (2008) demonstrated a sharp drop in both $K_{Mg/Ca}$ and $K_{U/Ca}$ at linear extension rates below ~0.2 nm s^{-1}, accompanied by no significant change in the ratio between the two. Limited aragonite $K_{Li/Ca}$ experimental data confirm a positive growth rate effect, but it does not appear to be as strong as for $K_{Mg/Ca}$ (Gabitov et al., 2011), which would tend to drive the biogenic data off the isotherms. We infer from this that precipitation rate and degree of entrapment are unlikely to be *dominant* drivers of the biogenic Li/Mg observations, but additional abiotic growth rate experiments are required for confirmation. In the following we make the simplifying assumption of 100% entrapment, and we explore other potential biomineralization dynamics. We return to kinetics when discussing Sr/Ca in Section 3.6.

3.4. Hypothetical effect of Ca^{2+} pumping

The Mg/Ca and Li/Ca ratios observed in *H. elegans* and corals could be consistent with the abiotic partition coefficients predicted in Section 3.2 (i.e. with 100% entrapment) if Mg/Ca and Li/Ca ratios in the organisms' calcifying fluids are lower than those in seawater, with *H. elegans* being lowest of all. Calcifying organisms must exert tight controls over the precipitation of $CaCO_3$, and hence they create a 'privileged space' that is isolated from seawater. Since cytosolic $[Ca^{2+}]$ must be kept low (<1 μM) for cell health, vacuolized or extracellular seawater (10 mM $[Ca^{2+}]$) likely provides a baseline for the calcifying fluid (e.g. Erez, 2003). Seawater vacuolization, alkalization, and delivery to sites of calcification have been demonstrated in benthic foraminifera (Bentov et al., 2009; de Nooijer et al., 2009b). Corals sequester their calcifying fluid extracellularly against the skeleton (Adkins et al., 2003; McConnaughey, 1989) with tracers documenting at least some direct seawater transport to the site of calcification

229 (Gagnon et al., 2012; Tambutte et al., 2011). Once seawater is isolated and $CaCO_3$ precipitation
230 begins, Rayleigh fractionation will result in modification of the calcifying fluid's Mg/Ca and
231 Li/Ca ratios (Elderfield et al., 1996), but because Mg and Li are highly incompatible this process
232 is expected to raise, not lower, those ratios (Section 3.5). Therefore we require another
233 mechanism to lower Mg/Ca and Li/Ca in the calcifying fluid.

234 Mg^{2+} is well known to poison calcite precipitation (Berner, 1975), and it has been suggested
235 that foraminifera actively pump Mg^{2+} out of their privileged spaces in order to precipitate low-
236 Mg calcite (Bentov and Erez, 2006). Such a process could explain our observations if Mg^{2+}
237 pumps also export Li^+ with essentially no discrimination, but this seems unlikely given their
238 different valence states. Furthermore the Mg^{2+} pumping strategy has been shown to be
239 energetically inferior to raising calcifying fluid pH via H^+ export (Zeebe and Sanyal, 2002), and
240 in fact aragonitic organisms have no specific need to exclude Mg^{2+}. Li^+ export would likely
241 impart a large isotopic fractionation given the low masses of its isotopes (^6Li and ^7Li), yet
242 calcitic foraminifera and aragonitic corals exhibit similar δ^7Li to their respective abiotic
243 precipitates (Marriott et al., 2004a).

244 We therefore consider Ca^{2+} import as an alternative, with transmembrane pumps (or
245 channels) that discriminate almost completely against both Mg^{2+} and Li^+. Mg^{2+} and Li^+ ionic
246 radii are small compared to Ca^{2+}, which might explain the specificity of a Ca^{2+} pump. Ca^{2+}
247 pumping carries the advantage of raising pH in the privileged space, thereby promoting $CaCO_3$
248 precipitation (McConnaughey, 1989; Zeebe and Sanyal, 2002; Sinclair and Risk, 2006). Active
249 concentration of Ca^{2+} may also be required to satisfy known biomineralization rates. Allison et
250 al. (2011) calculated that the coral *Galaxea fascicularis* would need to empty and refill its
251 privileged space at least 10,000 times per hour if all of its Ca^{2+} were supplied from unmodified

252 seawater. Similarly, de Nooijer et al. (2009a) estimated that the calcitic benthic foraminifer
253 *Ammonia aomoriensis* must process ~75 times its own volume in seawater to obtain enough Ca^{2+}
254 to build a single chamber, yet vacuole turnover was observed to be far too slow to accommodate
255 that need. These observations could implicate the existence of large internal stores of Ca^{2+},
256 perhaps in a solid form like amorphous $CaCO_3$ (ACC) (Erez, 2003). However, recent *in vitro*
257 tracer experiments with *A. aomoriensis* led Nehrke et al. (2013) to conclude that the main source
258 of Ca^{2+} is not vacuolized seawater, nor some internal Ca^{2+} store like ACC, but rather it is
259 delivered directly to the privileged space via pumping from seawater. Some vacuolized seawater
260 does still reach the site of calcification, and most or all of the Mg^{2+} and Li^{+} that ends up in the
261 mineral would be supplied by those vacuoles and/or by breaks in the cytoplasmic sheet covering
262 the privileged space (or by extracellular openings in the case of corals). Under this scenario the
263 spread along a Li/Mg isotherm can be considered as a two-component mixture between a
264 perfectly isolated privileged space (all Ca^{2+} actively pumped, represented by the origin in Fig. 4
265 if the pump completely discriminates against Mg^{2+} and Li^{+}) and passively incorporated seawater
266 (filled dots). This is numerically equivalent to pumping Ca^{2+} into a seawater-derived reservoir
267 (Sinclair and Risk, 2006), which would cause the chemistry in Figure 4 to migrate from the filled
268 dots toward the origin.

269 Inferred [Ca^{2+}] in the calcifying fluid can be derived by finding the fluid's Mg/Ca (or Li/Ca)
270 ratio that is required for the biogenic aragonite data to be compatible with the abiotic partition
271 coefficients, while leaving fluid [Mg^{2+}] and [Li^{+}] at their seawater values. The constraint of using
272 abiotic partition coefficients is an important difference from previous models that used empirical
273 biogenic partition coefficients (especially critical for Mg), allowing them to match coral
274 chemistry using minimal elevations of fluid [Ca^{2+}] (Sinclair and Risk, 2005; Gagnon et al., 2007,

2012). In contrast, our inferred [Ca^{2+}] ranges from ~13 mM (~30% enrichment over seawater) for the warmest corals to >400 mM (~40-fold enrichment) for the coldest *H. elegans* (Fig. 4). Ca^{2+}-ATPases, which exchange Ca^{2+} for H^+, have been implicated in various calcifying plants and animals and have been characterized in the coral *Stylophora pistillata* (Zoccola et al., 2004). Ca^{2+}-ATPase can maintain a cross-membrane [Ca^{2+}] gradient of order 10,000-100,000-fold (Langer et al., 2006), so our inferred concentrations are feasible if pumped directly from seawater or an intermediary Ca^{2+} pool, and not adjacent to cytosol. The biogenic aragonite data imply that less pumping generally occurs in warmer waters, hypothetically due to higher aragonite saturation states. Microsensor measurements document elevated [Ca^{2+}] in the calcifying fluid of the coral *G. fascicularis*, but at levels much more modest than inferred here (Al-Horani et al., 2003). We note, however, that our inferred Ca^{2+} concentrations need not be free in the calcifying fluid, but could be largely sequestered in ACC or organic ligands, which would also alleviate the thermodynamic limit of Ca^{2+}-ATPase. In that light the extreme accumulation of Ca^{2+} would be less a requirement of raising the saturation state and more a material necessity of house building (Nehrke et al., 2013). In fact, very high free [Ca^{2+}] (and hence pH) does not necessarily translate into higher aragonite precipitation rates, because the carbon supply may become limited by the CO_2 diffusion rate across membranes at zero CO_2 in the privileged space (Sinclair and Risk, 2006).

If the bulk of the Ca^{2+} precipitated into aragonite is acquired by pumping, then an isotopic fractionation would be expected because transmembrane transport likely discriminates against heavier isotopes. Coccolithophores (Gussone et al., 2006) and corals (Böhm et al., 2006) exhibit similar $\delta^{44/40}Ca$ despite an offset of ~0.6‰ between inorganic calcite and aragonite (Gussone et al., 2005), suggesting a characteristic biological fractionation and no mineralogical fractionation

298 (Böhm et al., 2006; Gussone et al., 2006). *H. elegans* $\delta^{44/40}$Ca is slightly more depleted than
299 coccolithophores and corals, which might be consistent with a different level of transmembrane
300 transport (Gussone et al., 2016). It must be noted, however, that other processes can impart
301 isotopic fractionations during biomineralization, so the $\delta^{44/40}$Ca observations cannot be taken as
302 conclusive evidence for or against Ca^{2+} pumping (Gussone et al., 2016).
303
304 **3.5. Rayleigh fractionation**
305 If *H. elegans* and corals calcify from a calcifying fluid that is isolated from seawater, then
306 depletion of the Ca^{2+} in that pool will result in Rayleigh fractionation of the various cations
307 present, given mathematically by Elderfield et al. (1996). This process has been implicated in
308 explaining why calcitic benthic foraminiferal trace element ratios tend to vary with calcite
309 saturation state, with lower saturation leading to a more isolated (infrequently replenished)
310 reservoir and hence greater fractionations (Elderfield et al., 1996). It has also been included in
311 various attempts to explain coral trace element ratios (e.g. Case et al., 2010; Gaetani et al., 2011;
312 Gagnon et al., 2007; Montagna et al., 2014). The case for Li^{+} and Mg^{2+} is simple because the
313 abiotic aragonite partition coefficients for these elements are <<1 (Gaetani and Cohen, 2006;
314 Marriott et al., 2004a). Therefore as calcification proceeds from a closed pool, [Ca^{2+}] declines
315 while [Li^{+}] and [Mg^{2+}] remain nearly constant (Case et al., 2010). This has almost exactly the
316 opposite effect of Ca^{2+} pumping: Li/Ca and Mg/Ca ratios in the privileged space rise, and
317 aragonite chemistry moves away from the origin, approximately along Li/Mg isotherms and with
318 little resulting impact on the Li/Mg thermometer (Fig. 4b). For 95% precipitation of the Ca^{2+}
319 pool (f = 0.05), Li/Mg deviations away from isotherms range from ~0.6% at the warm end to
320 ~6% at the cold end, regardless of the [Ca^{2+}] starting point.

3.6. Is Sr/Ca consistent with this model?

Much work has been devoted to understanding Sr/Ca in corals because of its utility as a paleotemperature proxy (see Cohen and Gaetani, 2010, for a review). Here we simply examine what is required for paired Sr/Ca and Mg/Ca data to fit within the confines of our biomineralization model. The lack of a positive correlation between Sr/Ca and Mg/Ca in corals at a given temperature (Fig. 5a) indicates that in contrast to Li/Mg, Sr/Mg ratios in the privileged space are not constant. This in turn could mean two things: the Ca^{2+} pump could be 'leaky' with respect to Sr^{2+}, and/or Rayleigh fractionation may be important. To evaluate the relative impacts of these two effects we use abiotic aragonite $K_{Sr/Ca}$ from Gaetani and Cohen (2006), who found a decrease with temperature (r^2=0.97) in good agreement with Kinsman and Holland (1969). $K_{Sr/Ca}$ is slightly above 1 at oceanic temperatures, much higher than $K_{Mg/Ca}$, indicating that Rayleigh fractionation is likely to be important for Sr/Mg. In Figure 5a we show pre-Rayleigh trajectories for paired Sr/Ca and Mg/Ca at a single arbitrary temperature (12°C) assuming [Ca^{2+}] in the privileged space is raised by a pump that has various levels of affinity for Sr^{2+}. An affinity value of 1 means that the pump makes no distinction between the two elements and therefore transports them at the seawater ratio, while values lower than 1 indicate that Sr^{2+} is less efficiently transported than Ca^{2+}. This model only projects into the range of the coral data if there is little discrimination. Since any Rayleigh fractionation will drive aragonite Sr/Ca lower, a Sr^{2+} to Ca^{2+} transport stoichiometry of ~0.97 could be an approximate lower limit that satisfies nearly all of the data (Fig. 5b). A value that high is mainly constrained by the cold-end coral data where abiotic $K_{Sr/Ca}$ and $K_{Mg/Ca}$ are less certain (Gaetani and Cohen, 2006), while warm water data can accommodate a stoichiometry as low as ~0.9. Berman and King (1990) reported Sr:Ca transport

stoichiometries of 0.82-0.93 in Ca^{2+}-ATPase from rabbit muscle tissue, so our inferred values appear to be reasonable. This contrasts with the coral models of Sinclair and Risk (2006) and Gagnon et al. (2012), who assumed a pump that is impervious to Sr^{2+}.

In modifying a calcifying fluid that has experienced Ca^{2+} and Sr^{2+} pumping, Rayleigh fractionation will drive aragonite Sr/Ca down and Mg/Ca up, with trajectories shown as dashed lines in Figure 5a for 12°C and two arbitrary starting points. The spread of coral Sr/Ca and Mg/Ca data from a given temperature bin appears to run quasi-parallel to these trajectories, in support of this mechanism (Gagnon et al., 2007). Different coral specimens at a given temperature likely have different Rayleigh starting points due to variable amounts of pumping, leading to additional spread in the sub-horizontal direction in Figure 5. Rayleigh trajectories vary with not only with starting point chemistry (Fig. 5a) but also with temperature due to its impact on $K_{Sr/Ca}$ (Fig. 5b). The coral data appear to follow the predicted slopes at different temperatures (e.g. *Desmophyllum* at 3-6°C vs. *Acropora* at 27-30°C), further supporting the Rayleigh model and also the applicability of the abiotic $K_{Sr/Ca}$.

The Sr/Ca and Mg/Ca measurements in Figure 5 primarily represent fibrous aragonite, but some samples may hypothetically include admixtures of COC aragonite. If systemic, such admixtures could contribute to the observed horizontal scatter because COCs are consistently elevated in Mg/Ca (and Li/Ca) but not in Sr/Ca (Meibom et al., 2004; Gagnon et al., 2007; Montagna et al., 2014). As noted above, this could be related to greater Mg^{2+} and Li^{+} entrapment in faster growing COCs, whereas limited abiotic aragonite observations suggest that Sr^{2+} may be insensitive to entrapment over coral-relevant growth rates (Gabitov et al., 2006; Holcomb et al., 2009).

366 In contrast to corals, Sr/Ca and Mg/Ca in *H. elegans* are positively correlated, and both tend
367 to increase with temperature (Rosenthal et al., 2006). This is surprising given the inverse
368 relationship between Sr/Ca and temperature in both abiotic and coral aragonite. *H. elegans*
369 Sr/Mg behavior is, in fact, more akin to Li/Mg than to coral Sr/Mg (Fig. 6). This may indicate
370 that Ca^{2+} pumping discriminates more strongly against Sr^{2+} in *H. elegans*, and a Sr^{2+} to Ca^{2+}
371 transport stoichiometry of ~0.2-0.3 results in a reasonably good fit to the data. This model
372 therefore requires a great deal of pumping but relatively little Rayleigh fractionation, which
373 would drive values to the right in Figure 6. It furthermore suggests that the empirical correlations
374 between Sr/Ca, Mg/Ca, and temperature in *H. elegans* are actually dominated by the amount of
375 pumping, with greater pumping in colder waters. Much of the correlation to temperature may
376 actually be spurious because temperature is well correlated to seawater ΔCO_3^{2-} with respect to
377 aragonite in these data sets (Rosenthal et al., 2006), and indeed a dominant role for ΔCO_3^{2-} has
378 been implicated (Yu et al., 2014). Rosenthal et al. (2006) suggested that the ΔCO_3^{2-} influence is
379 limited to saturation states below ~15 µmol kg^{-1}, with temperature prevailing above that level.
380 According to our model the apparent ΔCO_3^{2-} effect may be explained by greater Ca^{2+} pumping in
381 less saturated waters (<15 µmol kg^{-1} is shown as triangles in Fig. 6), and it probably extends
382 above 15 µmol kg^{-1} albeit with a weaker influence (circles in Fig. 6). The predicted temperature
383 influence on *H. elegans* paired Sr/Ca and Mg/Ca is overwhelmed by Ca^{2+} pumping and Rayleigh
384 fractionation according to this model.
385 Alternatively the positive correlation between Sr/Ca and Mg/Ca in *H. elegans* could be a
386 consequence of surface entrapment due to slow but variable precipitation rates. The differing
387 behavior between organisms would require $K_{Sr/Ca}$ to be insensitive to the precipitation rates
388 found in corals (Gabitov et al., 2006; Holcomb et al., 2009), but sensitive to lower rates

hypothetically found in *H. elegans*. In that case some of the coral Mg/Ca lowering at near-constant Sr/Ca (Fig. 5) could be attributable to reduced Mg entrapment instead of Ca^{2+} pumping. The *H. elegans* Sr/Ca and Mg/Ca pattern (Fig. 6) might then accommodate a Ca^{2+} pump with a high affinity for Sr^{2+} (pushing chemistry to the left as in Fig. 5a), combined with Rayleigh fractionation (pushing chemistry to the right as in Fig. 6b). The observed correlation between Sr/Ca and temperature (Rosenthal et al., 2006) could again be spurious and due to the co-varying ΔCO_3^{2-}, with lower precipitation rates and less entrapment in undersaturated waters. We reiterate, however, that this scenario also requires the ratio between $K_{Li/Ca}$ and $K_{Mg/Ca}$ to remain nearly constant at a given temperature as growth rates vary, to satisfy the requirement that paired biogenic Li/Ca and Mg/Ca data remain along isotherms (Figs. 2, 4a), whereas limited experimental data suggest that is not the case (Gabitov et al., 2011).

3.7. Implications for paleotemperature estimation

We agree with prior workers (Bryan and Marchitto, 2008; Montagna et al., 2014; Raddatz et al., 2013) that Li/Mg is a promising paleotemperature proxy in *H. elegans* and various corals. If our hypothesis is correct, then Li/Mg may effectively account for 'vital effects' associated with organisms' modification of their calcifying fluids, e.g. in response to seawater ΔCO_3^{2-}. This could lead to greater paleotemperature accuracy (since ancillary parameters like ΔCO_3^{2-} need not be known) and precision (if the model is a reasonably complete description of biomineralization). The proxy is clearly not perfect however, as instances of anomalous Li/Mg ratios have been demonstrated in a portion of a *Porites* record from Japan (Hathorne et al., 2013) and between forereef and backreef *Siderastrea* from Belize (Fowell et al., 2016). The hypothetical influence of crystal growth rate on cation entrapment might account for some of the

observed scatter around our simple model, and thereby place limits on both accuracy and precision. If that is the case, then in corals it would be important to avoid mixing fibrous aragonite and faster growing COCs when generating temperature reconstructions (Montagna et al., 2014).

The standard errors of estimate for Li/Mg range from 0.22 mmol mol^{-1} for corals (Equation 2) to 0.29 mmol mol^{-1} for *H. elegans* (Equation 1). At cold temperatures where the relationship is steepest this translates to slightly better than ±1°C uncertainty, while at the warm end it balloons to several degrees. However, this analysis does not account for the fact that Li/Mg scatter is decreased in warm waters compared to cold waters, which counteracts the effect of the exponential response (Fig. 1c). Regressing the data with temperature as the dependent variable yields standard errors of estimate of 1.3°C (*H. elegans*) to 1.5°C (corals), which we take to be better measures of the temperature uncertainty.

We note that the cold-end scatter is substantially reduced if we regress Mg/Li (rather than Li/Mg) against temperature, but this also puts the flat part of the exponential curve in cold waters, negating the apparent gain in sensitivity (Fig. 7). Alternatively fitting *H. elegans* Mg/Li with a second-order polynomial produces an equation that is relatively steep at the cold end:

$$Mg/Li = 0.150 \pm 0.012 + 0.0209 \pm 0.0027T - 0.0002 \pm 0.0001T^2 \quad (5)$$

with $r^2 = 0.95$. Since the shape of this response is substantially different from the polynomial fit to the coral Mg/Li data (which is virtually identical to the coral exponential fit), we favor the exponential fits as better descriptors of the fundamental similarity between *H. elegans* and coral aragonite. However, preliminary downcore measurements suggest that *H. elegans* Equation (5) provides more realistic deep sea temperatures than Equation (1), so Equation (5) may serve as an empirically superior choice for paleotemperature reconstruction until additional calibration data

become available. The standard error of estimate for Mg/Li according to Equation (5) is 0.022 mol $mmol^{-1}$, which translates to ±1.0°C at 0°C and ±1.7°C at 20°C.

Some of the scatter in our compilations could further be related to combining data from different laboratories that are not intercalibrated or that employ different cleaning procedures, and some could be due to imprecise knowledge of calcification temperatures, so true precision might be better. In the deep ocean where reliable paleotemperature proxies are lacking, uncertainties of ~1°C would represent a step forward. If the overall Li/Mg error is random, then repeated measurements on the same samples could reduce the paleotemperature uncertainty below 1°C.

It is tempting to try extending our biomineralization model to calcitic foraminifera. For several calcitic benthic foraminiferal taxa, Mg/Li is strongly correlated to temperature (r^2 = 0.71-0.90) but this represents only a slight improvement over Mg/Ca, in contrast to the case for *H. elegans* (Bryan and Marchitto, 2008). Importantly, different calcitic taxa yield significantly distinct Mg/Li slopes and intercepts, implying that additional unknown factors must be affecting their Mg/Li ratios. Langer et al. (2015) proposed that Ca^{2+} channels in *Amphistegina lessonii* are more permeable to Li^{+} than to Mg^{2+}, which would cause calcite Mg/Li to vary somewhat with the extent of pumping at a given temperature. For planktonic foraminifera there is no apparent correlation between Mg/Ca and Li/Ca within a given temperature range (Allen et al., 2016). This latter observation is reassuring for the use of Mg/Ca as a temperature proxy, as it suggests that Ca^{2+} pumping (with Mg^{2+} and Li^{+} exclusion) is not so important for planktonic foraminifera. We conclude that our simple biomineralization model and its implications for Li/Mg-based temperature reconstruction are only directly applicable to certain biogenic aragonites.

457 The impact of Rayleigh fractionation on the coral Sr/Ca thermometer has been noted
458 previously (e.g. Gaetani and Cohen, 2006; Gagnon et al., 2007). The relationship between Sr/Ca
459 and temperature can vary between different taxa, different localities, and even different growth
460 axes on the same coral head (e.g. de Villiers et al., 1995; Marshall and McCulloch, 2002;
461 Corrège, 2006). These variations may be attributable to differing amounts of Rayleigh
462 fractionation. The impact of Ca^{2+} pumping on the Sr/Ca thermometer appears to be
463 comparatively smaller because of the pump's high affinity for Sr^{2+} (Fig. 5b). We encourage the
464 continued use of multiple elements to isolate the temperature signal, whether it be Li/Mg, Mg-Sr-
465 Ba (Gaetani et al., 2011), U/Sr (DeCarlo et al., 2016), or some other combination.
466
467 **4. Conclusions**
468 We present a simple conceptual model that explains the remarkably similar behavior of
469 Li/Mg between the aragonitic foraminifer *H. elegans* and various aragonitic coral taxa. We
470 suggest that Li/Mg reflects the ratio between the abiotic partition coefficients $K_{Li/Ca}$ and $K_{Mg/Ca}$
471 because neither Ca^{2+} pumping nor Rayleigh fractionation significantly alters the Li/Mg ratio of
472 the calcifying fluid. This model is consistent with coral Sr/Ca if the Ca^{2+} pump barely
473 discriminates against Sr^{2+}. In contrast *H. elegans* Sr/Ca appears to require either a large
474 discrimination against pumping Sr^{2+}, or an important role for aragonite precipitation rate through
475 its impact on surface cation entrapment. In either case Li/Mg appears to be largely unaffected by
476 such 'vital effects,' and therefore it holds unusual promise as a paleotemperature proxy.
477
478 **Acknowledgments**

We are grateful to Matthias López Correa and Andres Rüggeberg for providing access to the cold-water coral samples listed in Table 2, as well as to Riccardo Rodolfo-Metalpa for the *Cladocora caespitosa* samples. We thank Derek Weller for laboratory assistance. Ed Hathorne and an anonymous reviewer provided comments that improved this paper. This work was supported in part by US NSF grants OCE-0425522 and OCE-0648215 to Marchitto.

References

Adkins, J.F., Boyle, E.A., Curry, W.B., Lutringer, A., 2003. Stable isotopes in deep-sea corals and a new mechanism for "vital effects". Geochim. Cosmochim. Acta 67, 1129-1143.

Al-Horani, F.A., Al-Moghrabi, S.M., de Beer, D., 2003. The mechanism of calcification and its relation to photosynthesis and respiration in the scleractinian coral Galaxea fascicularis. Marine Biology 142, 419-426.

Allen, K.A., Hönisch, B., Eggins, S.M., Haynes, L.L., Rosenthal, Y., Yu, J., 2016. Trace element proxies for surface ocean conditions: A synthesis of culture calibrations with planktic foraminifera. Geochim. Cosmochim. Acta 193, 197-221.

Allison, N., Finch, A.A., 2010. $\delta^{11}B$, Sr, Mg and B in a modern Porites coral: the relationship between calcification site pH and skeletal chemistry. Geochim. Cosmochim. Acta 74, 1790-1800.

Allison, N., Cohen, I., Finch, A.A., Erez, J., 2011. Controls on Sr/Ca and Mg/Ca in scleractinian corals: The effects of Ca-ATPase and transcellular Ca channels on skeletal chemistry. Geochim. Cosmochim. Acta 75, 6350-6360.

Beck, J.W., Edwards, R.L., Ito, E., Taylor, F.W., Recy, J., Rougerie, F., Joannot, P., Henin, C., 1992. Sea-surface temperature from coral skeletal strontium/calcium ratios. Science 257, 644-647.

Bentov, S., Brownlee, C., Erez, J., 2009. The role of seawater endocytosis in the biomineralization process in calcareous foraminifera. Proceedings of the National Academy of Sciences of the United States of America 106, 21500-21504.

506 Bentov, S., Erez, J., 2006. Impact of biomineralization processes on the Mg content of
507 foraminiferal shells: A biological perspective. Geochemistry, Geophysics, Geosystems 7,
508 Q01P08, doi:10.1029/2005GC001015.
509 Berman, M.C., King, S.B., 1990. Stoichiometries of calcium and strontium transport coupled to
510 ATP and acetyl phosphate hydrolysis by skeletal sarcoplasmic reticulum. Biochimica et
511 Biophysica Acta (BBA) - Biomembranes 1029, 235-240.
512 Berner, R.A., 1975. The role of magnesium in the crystal growth of calcite and aragonite from
513 sea water. Geochim. Cosmochim. Acta 39, 489-504.
514 Böhm, F., Gussone, N., Eisenhauer, A., Dullo, W.-C., Reynaud, S., Paytan, A., 2006. Calcium
515 isotope fractionation in modern scleractinian corals. Geochim. Cosmochim. Acta 70, 4452-
516 4462.
517 Boyle, E.A., Rosenthal, Y., 1996. Chemical hydrography of the South Atlantic during the last
518 glacial maximum: Cd vs. $d^{13}C$, in: Wefer, G., al., e. (Eds.), The South Atlantic: Present and
519 Past Circulation. Springer-Verlag, Berlin, pp. 423-443.
520 Brahmi, C., Kopp, C., Domart-Coulon, I., Stolarski, J., Meibom, A., 2012. Skeletal growth
521 dynamics linked to trace-element composition in the scleractinian coral Pocillopora
522 damicornis. Geochim. Cosmochim. Acta 99, 146-158.
523 Bryan, S.P., Marchitto, T.M., 2008. Mg/Ca-temperature proxy in benthic foraminifera: New
524 calibrations from the Florida Straits and a hypothesis regarding Mg/Li. Paleoceanography 23,
525 PA2220, doi:2210.1029/2007PA001553.
526 Case, D.H., Robinson, L.F., Auro, M.E., Gagnon, A.C., 2010. Environmental and biological
527 controls on Mg and Li in deep-sea scleractinian corals. Earth and Planetary Science Letters
528 300, 215-225.

529 Cohen, A.L., Gaetani, G.A., 2010. Ion Partitioning and the Geochemistry of Coral Skeletons:
530 Solving the Mystery of the “Vital Effect”, in: Prieto, M., Stoll, H.M. (Eds.), On partitioning
531 in low temperature aqueous systems: from fundamentals to applications in climate proxies
532 and environmental geochemistry.
533 Correge, 2006. Sea surface temperature and salinity reconstruction from coral geochemical
534 tracers. Palaeogeography, Palaeoclimatology, Palaeoecology 232, 408-428.
535 de Nooijer, L.J., Langer, G., Nehrke, G., Bijma, J., 2009a. Physiological controls on seawater
536 uptake and calcification in the benthic foraminifer Ammonia tepida. Biogeosciences 6, 2669-
537 2675.
538 de Nooijer, L.J., Toyofuku, T., Kitazato, H., 2009b. Foraminifera promote calcification by
539 elevating their intracellular pH. Proceedings of the National Academy of Sciences 106,
540 15374-15378.
541 de Villiers, S., Nelson, B.K., Chivas, A.R., 1995. Biological-Controls On Coral Sr/Ca And
542 Delta-O-18 Reconstructions Of Sea-Surface Temperatures. Science 269, 1247-1249.
543 DeCarlo, T.M., Gaetani, G.A., Cohen, A.L., Foster, G.L., Alpert, A.E., Stewart, J.A., 2016. Coral
544 Sr-U thermometry. Paleoceanography 31, 626-638.
545 Delaney, M.L., Be, A.W.H., Boyle, E.A., 1985. Li, Sr, Mg, And Na In Foraminiferal Calcite
546 Shells From Laboratory Culture, Sediment Traps, And Sediment Cores. Geochim.
547 Cosmochim. Acta 49, 1327-1341.
548 Elderfield, H., Bertram, C.J., Erez, J., 1996. A biomineralization model for the incorporation of
549 trace elements into foraminiferal calcium carbonate. Earth and Planetary Science Letters 142,
550 409-423.

551 Erez, J., 2003. The source of ions for biomineralization in foraminifera and their implications for
552 paleoceanographic proxies, in: Dove, P.M., DeYoreo, J.J., Weiner, S. (Eds.),
553 Biomineralization, pp. 115-149.
554 Finch, A.A., Allison, N., 2007. Coordination of Sr and Mg in calcite and aragonite.
555 Mineralogical Magazine 71, 539-552.
556 Finch, A.A., Allison, N., 2008. Mg structural state in coral aragonite and implications for the
557 paleoenvironmental proxy. Geophysical Research Letters 35, L08704.
558 Fowell, S.E., Sandford, K., Stewart, J.A., Castillo, K.D., Ries, J.B., Foster, G.L., 2016. Intrareef
559 variations in Li/Mg and Sr/Ca sea surface temperature proxies in the Caribbean reef-building
560 coral Siderastrea siderea. Paleoceanography 31, 1315-1329.
561 Gabitov, R.I., Cohen, A.L., Gaetani, G.A., Holcomb, M., Watson, E.B., 2006. The impact of
562 crystal growth rate on element ratios in aragonite: An experimental approach to
563 understanding vital effects. Geochim. Cosmochim. Acta 70, A187.
564 Gabitov, R.I., Gaetani, G.A., Watson, E.B., Cohen, A.L., Ehrlich, H.L., 2008. Experimental
565 determination of growth rate effect on U6+ and Mg2+ partitioning between aragonite and
566 fluid at elevated U6+ concentration. Geochim. Cosmochim. Acta 72, 4058-4068.
567 Gabitov, R.I., Schmitt, A.K., Rosner, M., McKeegan, K.D., Gaetani, G.A., Cohen, A.L., Watson,
568 E.B., Harrison, T.M., 2011. In situ d7Li, Li/Ca, and Mg/Ca analyses of synthetic aragonites.
569 Geochem. Geophys. Geosyst. 12, Q03001.
570 Gaetani, G.A., Cohen, A.L., 2006. Element partitioning during precipitation of aragonite from
571 seawater: A framework for understanding paleoproxies. Geochim. Cosmochim. Acta 70,
572 4617-4634.

573 Gaetani, G.A., Cohen, A.L., Wang, Z., Crusius, J., 2011. Rayleigh-based, multi-element coral
574 thermometry: A biomineralization approach to developing climate proxies. Geochim.
575 Cosmochim. Acta 75, 1920-1932.
576 Gagnon, A.C., Adkins, J.F., Erez, J., 2012. Seawater transport during coral biomineralization.
577 Earth and Planetary Science Letters 329–330, 150-161.
578 Gagnon, A.C., Adkins, J.F., Fernandez, D.P., Robinson, L.F., 2007. Sr/Ca and Mg/Ca vital
579 effects correlated with skeletal architecture in a scleractinian deep-sea coral and the role of
580 Rayleigh fractionation. Earth and Planetary Science Letters 261, 280-295.
581 Gussone, N., Böhm, F., Eisenhauer, A., Dietzel, M., Heuser, A., Teichert, B.M.A., Reitner, J.,
582 Wörheide, G., Dullo, W.-C., 2005. Calcium isotope fractionation in calcite and aragonite.
583 Geochim. Cosmochim. Acta 69, 4485-4494.
584 Gussone, N., Filipsson, H.L., Kuhnert, H., 2016. Mg/Ca, Sr/Ca and Ca isotope ratios in
585 benthonic foraminifers related to test structure, mineralogy and environmental controls.
586 Geochim. Cosmochim. Acta 173, 142-159.
587 Gussone, N., Langer, G., Thoms, S., Nehrke, G., Eisenhauer, A., Riebesell, U., Wefer, G., 2006.
588 Cellular calcium pathways and isotope fractionation in *Emiliania huxleyi*. Geology 34, 625-
589 628.
590 Hall, J.M., Chan, L.-H., 2004. Li/Ca in multiple species of benthic and planktonic foraminifera:
591 Thermocline, latitudinal, and glacial-interglacial variation. Geochim. Cosmochim. Acta 68,
592 529-545.
593 Hathorne, E.C., Felis, T., Suzuki, A., Kawahata, H., Cabioch, G., 2013. Lithium in the aragonite
594 skeletons of massive Porites corals: A new tool to reconstruct tropical sea surface
595 temperatures. Paleoceanography 28, 143-152.

596 Holcomb, M., Cohen, A.L., Gabitov, R.I., Hutter, J.L., 2009. Compositional and morphological
597 features of aragonite precipitated experimentally from seawater and biogenically by corals.
598 Geochim. Cosmochim. Acta 73, 4166-4179.
599 Inoue, M., Suzuki, A., Nohara, M., Hibino, K., Kawahata, H., 2007. Empirical assessment of
600 coral Sr/Ca and Mg/Ca ratios as climate proxies using colonies grown at different
601 temperatures. Geophysical Research Letters 34, n/a-n/a.
602 Kinsman, D.J.J., Holland, H.D., 1969. The co-precipitation of cations with CaCO3—IV. The co-
603 precipitation of Sr2+ with aragonite between 16° and 96°C. Geochim. Cosmochim. Acta 33,
604 1-17.
605 Langer, G., Gussone, N., Nehrke, G., Riebesell, U., Eisenhauer, A., Kuhnert, H., Rost, B.,
606 Trimborn, S., Thoms, S., 2006. Coccolith strontium to calcium ratios in Emiliania huxleyi:
607 The dependence on seawater strontium and calcium concentrations. Limnol. Oceanogr. 51,
608 310-320.
609 Langer, G., Sadekov, A., Thoms, S., Mewes, A., Nehrke, G., Greaves, M., Misra, S., Bijma, J.,
610 Elderfield, H., 2015. Li partitioning in the benthic foraminifera Amphistegina lessonii.
611 Geochemistry, Geophysics, Geosystems 16, 4275-4279.
612 Lear, C.H., Mawbey, E.M., Rosenthal, Y., 2010. Cenozoic benthic foraminiferal Mg/Ca and
613 Li/Ca records: Toward unlocking temperatures and saturation states. Paleoceanography 25,
614 PA4215.
615 Lear, C.H., Rosenthal, Y., 2006. Benthic foraminiferal Li/Ca: Insights into Cenozoic seawater
616 carbonate saturation state. Geology 34, 985-988.
617 López Correa, M.L., Montagna, P., Vendrell-Simón, B., McCulloch, M., Taviani, M., 2010.
618 Stable isotopes (δ18O and δ13C), trace and minor element compositions of Recent

619 scleractinians and Last Glacial bivalves at the Santa Maria di Leuca deep-water coral
620 province, Ionian Sea. Deep Sea Research Part II: Topical Studies in Oceanography 57, 471-
621 486.
622 Marchitto, T.M., 2006. Precise multi-elemental ratios in small foraminiferal samples determined
623 by sector field ICP-MS. Geochemistry, Geophysics, Geosystems 7, Q05P13,
624 doi:10.1029/2005GC001018.
625 Marriott, C.S., Henderson, G.M., Crompton, R., Staubwasser, M., Shaw, S., 2004a. Effect of
626 mineralogy, salinity, and temperature on Li/Ca and Li isotope composition of calcium
627 carbonate. Chem. Geol. 212, 5-15.
628 Marriott, C.S., Henderson, G.M., Belshaw, N.S., Tudhope, A.W., 2004b. Temperature
629 dependence of delta Li-7, delta Ca-44 and Li/Ca during growth of calcium carbonate. Earth
630 And Planetary Science Letters 222, 615-624.
631 Marshall, J.F., McCulloch, M.T., 2002. An assessment of the Sr/Ca ratio in shallow water
632 hermatypic corals as a proxy for sea surface temperature. Geochim. Cosmochim. Acta 66,
633 3263-3280.
634 McConnaughey, T., 1989. 13C and 18O isotopic disequilibrium in biological carbonates: II. In
635 vitro simulation of kinetic isotope effects. Geochim. Cosmochim. Acta 53, 163-171.
636 Meibom, A., Cuif, J.-P., Hillion, F., Constantz, B.R., Juillet-Leclerc, A., Dauphin, Y., Watanabe,
637 T., Dunbar, R.B., 2004. Distribution of magnesium in coral skeleton. Geophysical Research
638 Letters 31, L23306, doi:10.1029/2004GL021313.
639 Montagna, P., McCulloch, M., Douville, E., López Correa, M., Trotter, J., Rodolfo-Metalpa, R.,
640 Dissard, D., Ferrier-Pagès, C., Frank, N., Freiwald, A., Goldstein, S., Mazzoli, C., Reynaud,

641 S., Rüggeberg, A., Russo, S., Taviani, M., 2014. Li/Mg systematics in scleractinian corals:
642 Calibration of the thermometer. Geochim. Cosmochim. Acta 132, 288-310.
643 Montagna, P., McCulloch, M., Mazzoli, C., Silenzi, S., Odorico, R., 2007. The non-tropical coral
644 Cladocora caespitosa as the new climate archive for the Mediterranean: high-resolution
645 (~weekly) trace element systematics. Quaternary Science Reviews 26, 441-462.
646 Nehrke, G., Keul, N., Langer, G., de Nooijer, L.J., Bijma, J., Meibom, A., 2013. A new model
647 for biomineralization and trace-element signatures of Foraminifera tests. Biogeosciences 10,
648 6759-6767.
649 Nürnberg, D., 1995. Magnesium in tests of Neogloboquadrina pachyderma sinistral from high
650 northern and southern latitudes. The Journal of Foraminiferal Research 25, 350-368.
651 Raddatz, J., Liebetrau, V., Rüggeberg, A., Hathorne, E., Krabbenhöft, A., Eisenhauer, A., Böhm,
652 F., Vollstaedt, H., Fietzke, J., López Correa, M., Freiwald, A., Dullo, W.C., 2013. Stable Sr-
653 isotope, Sr/Ca, Mg/Ca, Li/Ca and Mg/Li ratios in the scleractinian cold-water coral Lophelia
654 pertusa. Chem. Geol. 352, 143-152.
655 Reynaud, S., Ferrier-Pagès, C., Meibom, A., Mostefaoui, S., Mortlock, R., Fairbanks, R.,
656 Allemand, D., 2007. Light and temperature effects on Sr/Ca and Mg/Ca ratios in the
657 scleractinian coral Acropora sp. Geochim. Cosmochim. Acta 71, 354-362.
658 Rollion-Bard, C., Blamart, D., 2015. Possible controls on Li, Na, and Mg incorporation into
659 aragonite coral skeletons. Chem. Geol. 396, 98-111.
660 Rosenthal, Y., Lear, C.H., Oppo, D.W., Linsley, B.K., 2006. Temperature and carbonate ion
661 effects on Mg/Ca and Sr/Ca ratios in benthic foraminifera: Aragonitic species *Hoeglundina*
662 *elegans*. Paleoceanography 21, PA1007, doi:1010.1029/2005PA001158.

663 Shirai, K., Kusakabe, M., Nakai, S., Ishii, T., Watanabe, T., Hiyagon, H., Sano, Y., 2005. Deep-
664 sea coral geochemistry: Implication for the vital effect. Chem. Geol. 224, 212-222.
665 Sinclair, D.J., Risk, M.J., 2006. A numerical model of trace-element coprecipitation in a
666 physicochemical calcification system: Application to coral biomineralization and trace-
667 element 'vital effects'. Geochim. Cosmochim. Acta 70, 3855-3868.
668 Tambutté, E., Tambutté, S., Segonds, N., Zoccola, D., Venn, A., Erez, J., Allemand, D., 2011.
669 Calcein labelling and electrophysiology: insights on coral tissue permeability and
670 calcification. Proceedings of the Royal Society B: Biological Sciences.
671 Watson, E.B., 2004. A conceptual model for near-surface kinetic controls on the trace-element
672 and stable isotope composition of abiogenic calcite crystals1. Geochim. Cosmochim. Acta
673 68, 1473-1488.
674 Wei, G., Sun, M., Li, X., Nie, B., 2000. Mg/Ca, Sr/Ca and U/Ca ratios of a porites coral from
675 Sanya Bay, Hainan Island, South China Sea and their relationships to sea surface
676 temperature. Palaeogeography, Palaeoclimatology, Palaeoecology 162, 59-74.
677 Xiao, Y., Liu, W., Ma, Y., Zhang, Y., He, M., Luo, C., Liao, Q., 2014. Correlation between δ
678 18O, Sr/Ca and Mg/Ca of coral Acropora and seawater temperature from coral culture
679 experiments. Sci. China Earth Sci. 57, 1048-1060.
680 Yu, J., Elderfield, H., Jin, Z., Tomascak, P., Rohling, E.J., 2014. Controls on Sr/Ca in benthic
681 foraminifera and implications for seawater Sr/Ca during the late Pleistocene. Quaternary
682 Science Reviews 98, 1-6.
683 Zeebe, R.E., Sanyal, A., 2002. Comparison of two potential strategies of planktonic foraminifera
684 for house building: Mg2+ or H+ removal? Geochim. Cosmochim. Acta 66, 1159-1169.

685 Zoccola, D., Tambutté, E., Kulhanek, E., Puverel, S., Scimeca, J.-C., Allemand, D., Tambutté,
686 S., 2004. Molecular cloning and localization of a PMCA P-type calcium ATPase from the
687 coral Stylophora pistillata. Biochimica et Biophysica Acta (BBA) - Biomembranes 1663,
688 117-126.
689
690

Table 1. New trace element measurements on core top *H. elegans* . Elemental ratios are given in mmol mol^{-1}, except Li/Ca which is in µmol mol^{-1}.

Core	Depth in core (cm)	Latitude	Longitude	Water depth (m)	Temperature (°C)	Li/Ca	Mg/Ca	Sr/Ca	Li/Mg
AII107-71GGC	5-7	31°31' S	35°56' W	1887	2.9	2.93	0.62	0.85	4.73
AII107-71GGC	5-7	31°31' S	35°56' W	1887	2.9	2.88	0.58	0.78	4.95
CHN82-15PC	0-6	43°22' N	28°14' W	2151	3.7	2.60	0.72	0.77	3.62
CHN82-15PC	0-6	43°22' N	28°14' W	2151	3.7	2.52	0.61	0.74	4.13
KNR166-2-16MC	0-1	24°24' N	83°14' W	248	10.8	3.87	1.41	2.32	2.75
KNR166-2-76MC	0-1	23°35' N	79°25' W	539	11.0	4.11	1.49	2.27	2.76
KNR166-2-89MC*	0-1	24°34' N	79°14' W	353	17.8	4.78	1.57	2.51	3.04
KNR166-2-123MC	0-1	24°46' N	79°16' W	632	10.6	3.58	1.30	2.18	2.75
RC13-140	10	2°52' N	87°45' W	2246	2.0	2.11	0.47	0.44	4.54
RC23-15	5	1°13' N	87°45' W	3612	2.0	1.39	0.26	0.45	5.35
RC23-22	10	1°00'N	83°37' W	3215	2.0	1.39	0.25	0.35	5.54

*3σ Li/Mg outlier omitted from figures

691

692

Table 2. Laser ablation ICP-MS Sr/Ca measurements (mmol mol^{-1}) made on fibrous aragonite from a subset of the corals in Montagna et al. (2014).

Sample code	Location	Latitude	Longitude	Depth (m)	Temperature (°C)	Species	Sr/Ca
Field specimens							
POS-325-433-1	Stjernsund, Norway	70°16' N	22°28' E	277-365	5.9	*Lophelia pertusa*	10.33
POS-325-433-2	Stjernsund, Norway	70°16' N	22°28' E	277-365	5.9	*Lophelia pertusa*	10.30
POS-228-216	Sula Ridge, Norway	64°07' N	8°07' E	250-320	7.52	*Lophelia pertusa*	10.15
POS-228-217	Sula Ridge, Norway	64°07' N	8°07' E	250-320	7.52	*Lophelia pertusa*	10.12
ALK-232-1050 BG	Oslofjord, Norway	59°06' N	10°41' E	105	8.2	*Lophelia pertusa*	9.88
DW13831#1	Darwin Mounds, UK	59°49' N	7°22' W	950	6.31	*Lophelia pertusa*	10.00
POS-292-544-1	Pelagia Mound, UK	55°31' N	15°40 W	835-858	7.92	*Lophelia pertusa*	9.91
POS-265-499	Propeller Mound, UK	52°09' N	12°46' W	729	9.6	*Lophelia pertusa*	9.93
VH-97-351	Galicia Bank, Spain	42°30' N	11°30' W	775-880	11.2	*Madrepora oculata*	10.22
M701-Dive111	Gondola Slide, Italy	41°44' N	17°03' E	674-710	13.55	*Lophelia pertusa*	9.76
M70-1-721-red	Santa Maria di Leuca, Italy	39°34' N	18°27' E	556-630	13.65	*Lophelia pertusa*	9.90
M70-1-721-white	Santa Maria di Leuca, Italy	39°34' N	18°27' E	556-630	13.65	*Lophelia pertusa*	9.84
M70-1-677	Urania Bank, Italy	36°50' N	13°09' E	440-654	13.65	*Lophelia pertusa*	10.06
GoM	Gulf of Mexico, US	29°10' N	88°01' W	434-465	9.3	*Lophelia pertusa*	10.22
N'Zeta	Offshore N'Zeta, Angola	7°17' S	12°03' E	370	8.72	*Lophelia pertusa*	9.96
Culturing experiments							
Clado-15					15.0	*Cladocora caespitosa*	9.60
Clado-18					18.0	*Cladocora caespitosa*	9.41
Clado-21					21.0	*Cladocora caespitosa*	9.14
Clado-23					23.0	*Cladocora caespitosa*	9.21

693
694

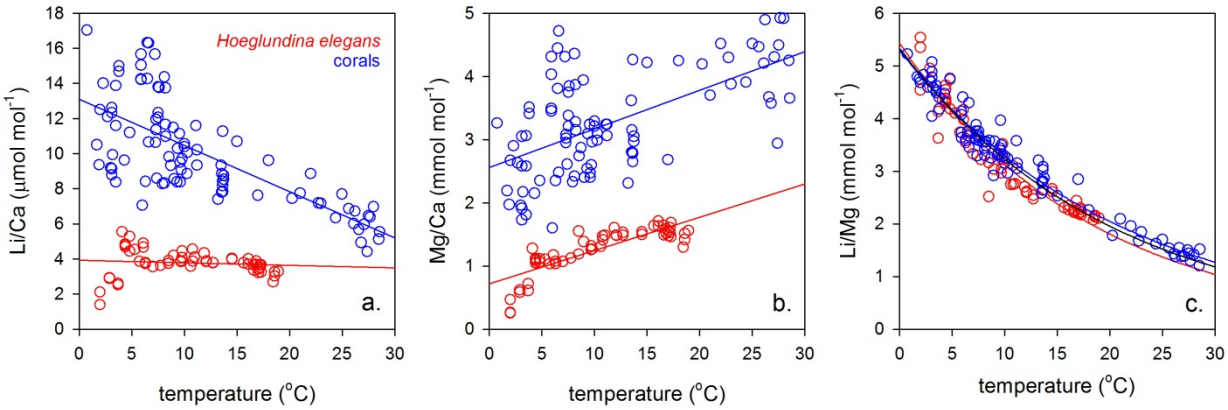

695

696

697 **Figure 1.** Li/Ca (**a.**), Mg/Ca (**b.**), and Li/Mg (**c.**) versus estimated growth temperature for the

698 aragonitic benthic foraminifer *H. elegans* (red) and various aragonitic coral taxa (blue). Fits

699 corresponding to Equations 1-3 are shown in panel (c.) in red, blue, and black, respectively.

700 References for published data are given in the text.

701

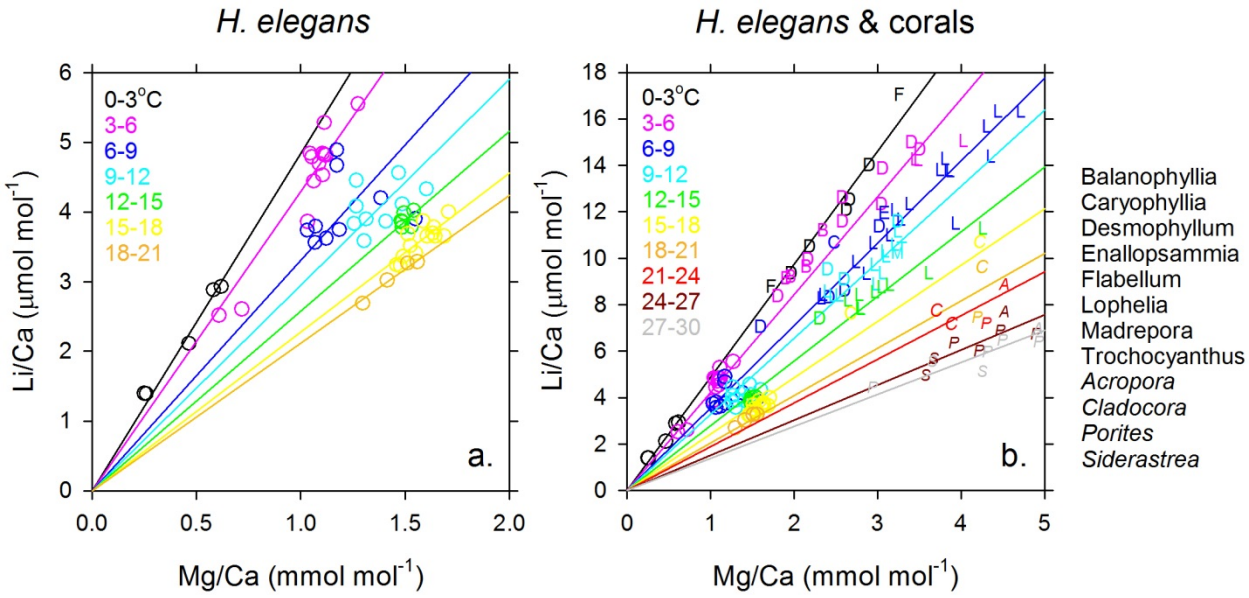

702

703

704 **Figure 2.** Li/Ca versus Mg/Ca in *H. elegans* (**a.**) and *H. elegans* combined with corals (**b.**). Data
705 are color-coded by growth temperature according to the legend, and lines are best fits for each
706 temperature bin, forced through the origin. Coral taxa are indicated using the first letter of the
707 genus, with deep sea corals in roman type and shallow hermatypic corals in italics. References
708 for published data are given in the text.

709

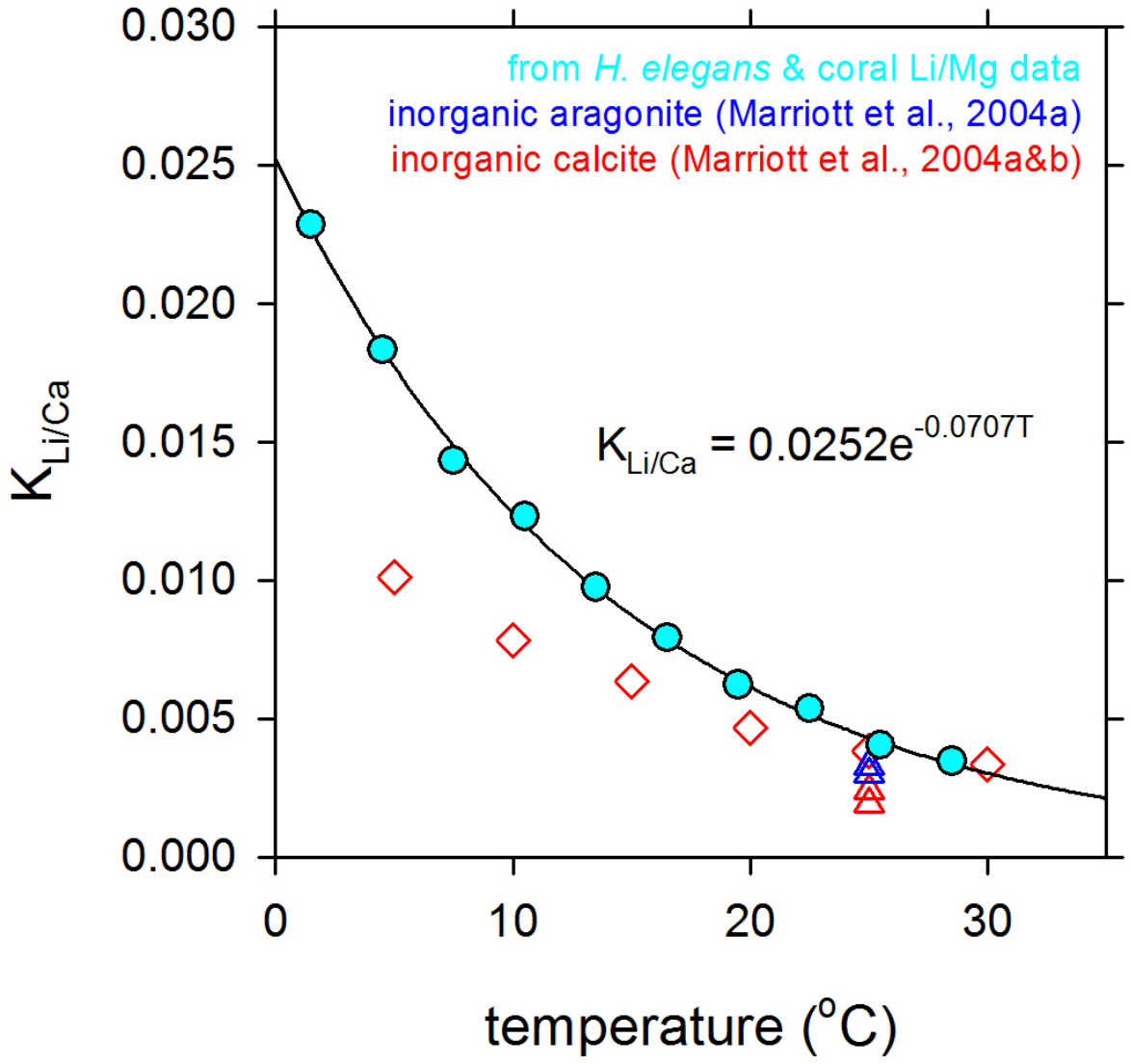

710

711

712 **Figure 3.** Predicted Li partition coefficients into aragonite as a function of temperature (cyan),
713 based on the *H. elegans* and coral Li/Mg regressions shown in Fig. 2b combined with the
714 temperature sensitivity of abiotic aragonite Mg partition coefficients from Gaetani and Cohen
715 (2006). Equation 4 is plotted in black. Data from abiotic aragonite (blue) and calcite (red) are
716 shown for comparison (Marriott et al., 2004a, b).

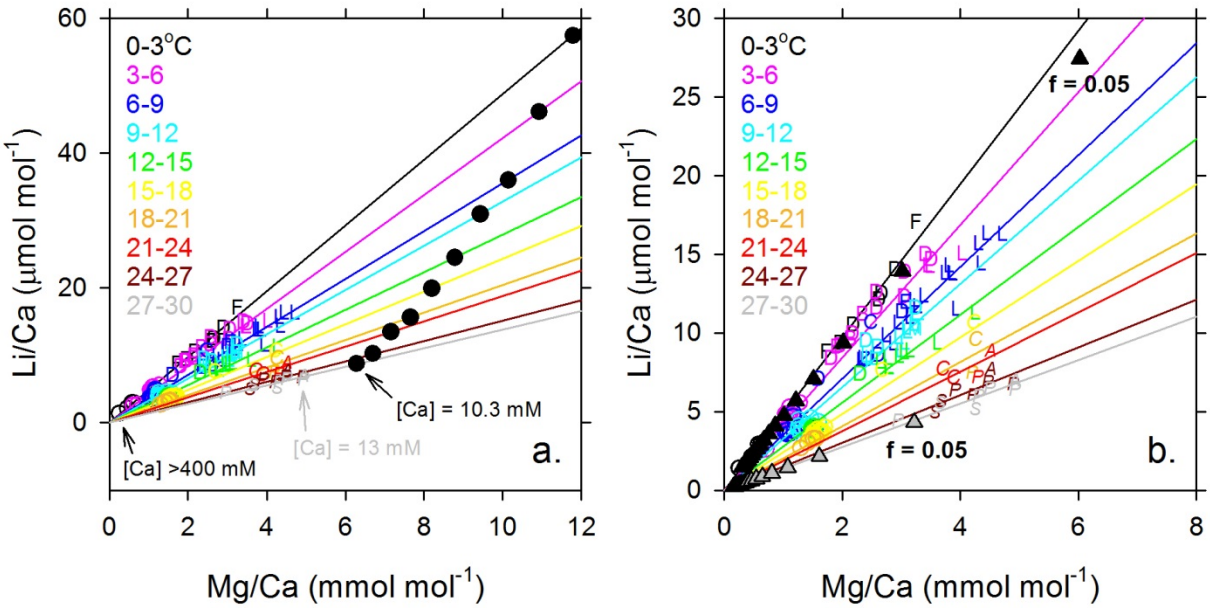

Figure 4. (**a.**) *H. elegans* and coral Li/Ca versus Mg/Ca as in Fig. 2b, but now including the composition of aragonite predicted if precipitated from unmodified seawater (black circles, plotted at the central temperature of each bin), based on the partition coefficients from Gaetani and Cohen (2006) and Fig. 3. The biogenic data may be explained by elevated Ca^{2+} within the calcifying fluid, and two extremes of the observations are indicated ($[Ca^{2+}]$ = 13 and >400 mM). (**b.**) As in (a.) but showing the effects of Rayleigh fractionation acting on a closed calcification pool (Elderfield et al., 1996) with an arbitrary initial $[Ca^{2+}]$ of 400 mM. Triangles show the evolution of aragonite away from the origin as f (fraction of initial Ca^{2+} remaining) declines in 0.05 increments, at 1.5°C (black) and 28.5°C (gray).

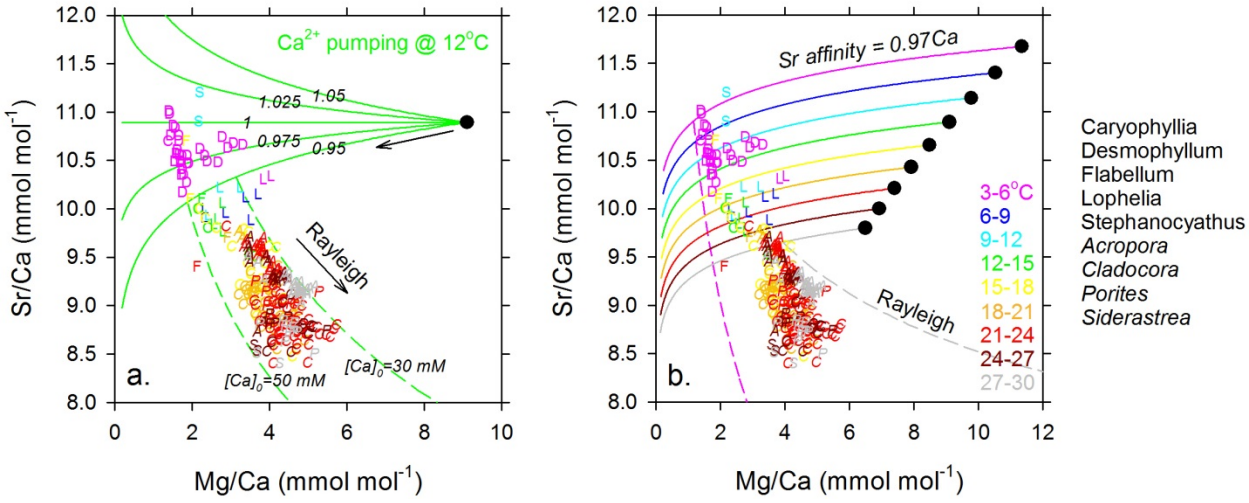

729

730

731 **Figure 5.** Coral Sr/Ca versus Mg/Ca, with taxa and growth temperatures coded as in Fig. 2b,
732 compared to aragonite precipitated from unmodified seawater at various temperatures (black
733 circles) based on the partition coefficients from Gaetani and Cohen (2006). (**a.**) Solid lines show
734 the impact of Ca^{2+} pumping, moving away from the seawater value at 12°C, assuming five
735 different hypothetical values for the pump's Sr:Ca transport stoichiometry. Rayleigh trajectories
736 are also shown (dashed lines) for two arbitrary initial Ca^{2+} concentrations (30 and 50 mM). (**b.**)
737 As in panel (a.) but showing pump trajectories over a range of temperatures with a Sr:Ca
738 transport stoichiometry of 0.97 (solid lines, plotted at the lowest temperature of each bin).
739 Rayleigh trajectories are plotted at 3°C and 27°C for two arbitrary initial Ca^{2+} concentrations
740 (dashed lines). Coral taxa are indicated using the first letter of the genus, with deep sea corals in
741 roman type and shallow hermatypic corals in italics. References for published data are given in
742 the text.

743

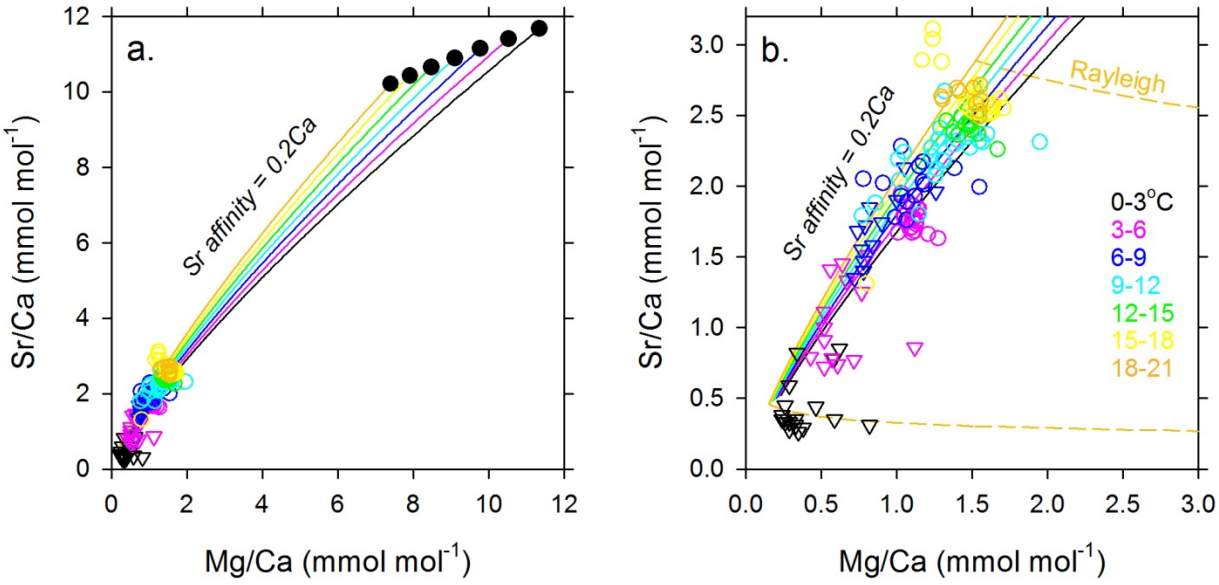

744

745

746 **Figure 6.** *H. elegans* Sr/Ca versus Mg/Ca, color coded by temperature as in previous figures,

747 with samples from <15 µmol kg^{-1} bottom water ΔCO_3^{2-} plotted as inverted triangles. (**a.**) Lines

748 show Ca^{2+} pumping trajectories away from aragonite precipitated from seawater (black circles)

749 assuming a Sr:Ca transport stoichiometry of 0.2 (plotted at the highest temperature of each bin).

750 (**b.**) As in panel (a.) but including Rayleigh trajectories at 21°C for two arbitrary initial Ca^{2+}

751 concentrations (dashed lines). References for published data are given in the text.

752

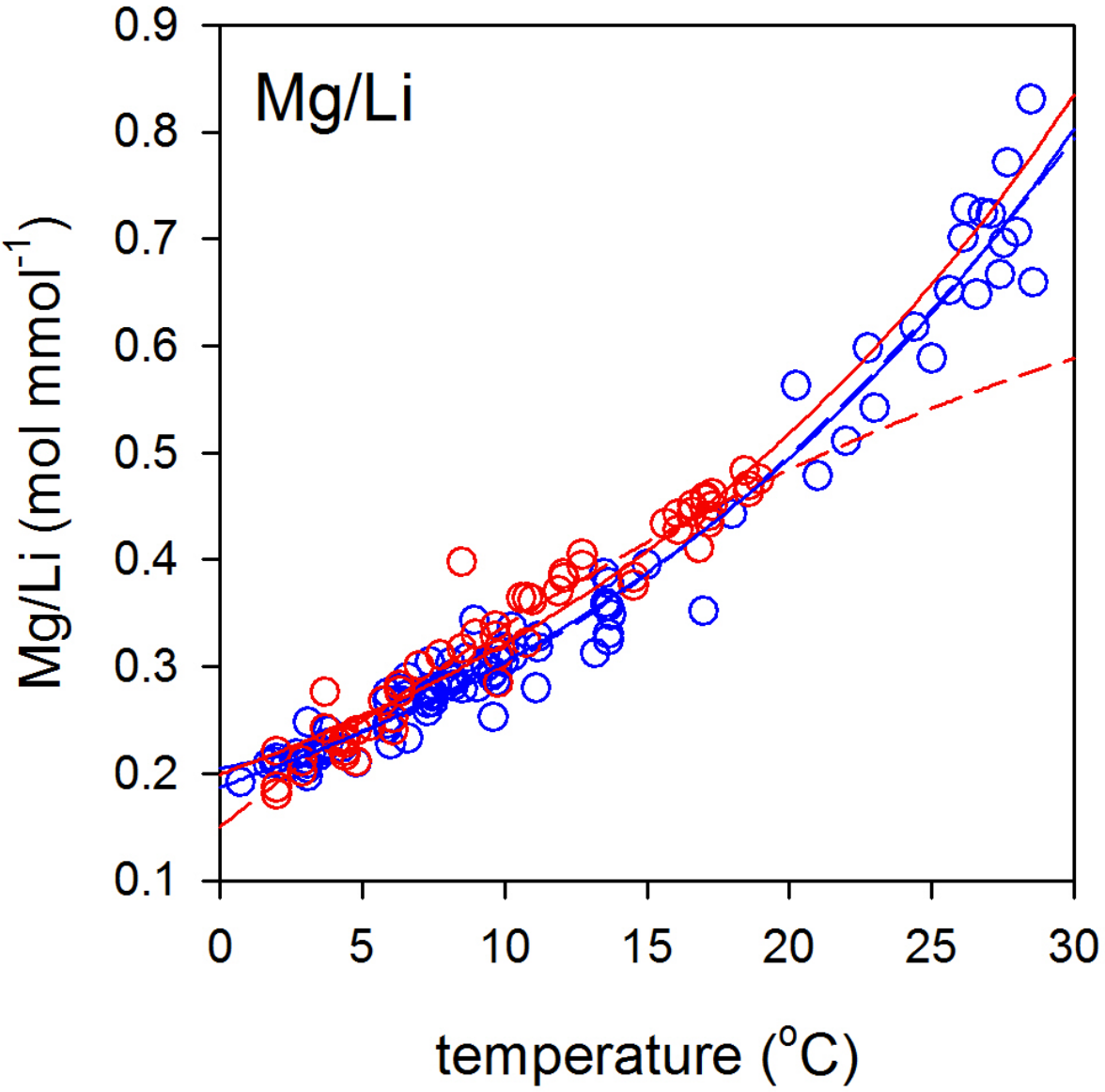

753

754

755 **Figure 7.** Mg/Li versus estimated growth temperature for the *H. elegans* (red) and various
756 aragonitic coral taxa (blue). The data are fit with exponentials (solid lines) and second-order
757 polynomials (dashed lines), including *H. elegans* Equation (5).